Surface-bound antigen induces B-cell permeabilization and lysosome exocytosis facilitating antigen uptake and presentation to T-cells

Fernando Y. Maeda[1#], Jurriaan J. H. van Haaren[1#], David B. Langley[2], Daniel Christ[2,3], Norma W. Andrews[1]* and Wenxia Song[1]*

[1]Department of Cell Biology and Molecular Genetics, University of Maryland, College Park, MD 20742, USA.

[2]Immunology Division, Garvan Institute of Medical Research, Darlinghurst, NSW 2010, Australia

[3]St Vincent's Clinical School, University of New South Wales, Darlinghurst, NSW 2010, Australia

[#]These authors contributed equally to this study.

*Co-corresponding authors:

Wenxia Song: wenxsong@umd.edu

Norma Andrews: andrewsn@umd.edu

Abstract

B-cell receptor (BCR)-mediated antigen internalization and presentation are essential for humoral memory immune responses. Antigen encountered by B-cells is often tightly associated with the surface of pathogens and/or antigen-presenting cells. Internalization of such antigens requires myosin-mediated traction forces and extracellular release of lysosomal enzymes, but the mechanism triggering lysosomal exocytosis is unknown. Here we show that BCR-mediated recognition of antigen tethered to beads, to planar lipid-bilayers or expressed on cell surfaces causes localized plasma membrane (PM) permeabilization, a process that requires BCR signaling and non-muscle myosin II. B-cell permeabilization triggers PM repair responses involving lysosomal exocytosis, and B-cells permeabilized by surface-associated antigen internalize more antigen than cells that remain intact. Higher affinity antigens cause more B-cell permeabilization and lysosomal exocytosis and are more efficiently presented to T-cells. Thus, PM permeabilization by surface-associated antigen triggers a lysosome-mediated B-cell resealing response, providing the extracellular hydrolases that facilitate antigen internalization and presentation.

Introduction

B-cells are responsible for generating antibody responses that neutralize pathogens and attract other immune cells. B-cell activation is initiated by the B-cell receptor (BCR), which surveys antigen through its membrane-anchored immunoglobulin (Reth 1994). Antigen-BCR interaction induces signaling cascades and antigen internalization, followed by intracellular processing and surface presentation to T-cells. Antigen presentation is essential for the activation of B-cells and their differentiation into high-affinity memory or antibody-secreting cells (Shlomchik and Weisel 2012). A property that is critical for maximizing humoral protection is the ability of clonal-specific BCRs to recognize antigens in their different physical, chemical, and biological forms.

Antigen encountered by B-cells *in vivo* is often tightly associated with the surface of pathogens, such as parasites, bacteria and viruses, and/or antigen-presenting cells, such as follicular dendritic cells (Gonzalez *et al.* 2011). Internalization, processing, and presentation of such surface-bound antigens are essential for specific B-cells to obtain T-cell help, which is critical for B-cell activation and differentiation. Follicular dendritic cells, which are uniquely present in germinal centers of secondary lymphoid organs, internalize antigens that drain into these organs and present them to B-cells (Suzuki *et al.* 2009; Cyster 2010). Competition between high and low-affinity B-cells to acquire antigen from follicular dendritic cells is a critical step in the selection of high-affinity B-cells that differentiate into memory B-cells and long-lived plasma cells.

B-cells, follicular B-cells in particular, are thought to have a limited ability to phagocytose large insoluble antigen particles (Vidard *et al.* 1996). However, B-cells are able to extract and

endocytose antigen that is tightly associated with non-internalizable surfaces (Batista and Neuberger 2000). Importantly, the efficiency by which B-cells present antigen depends more strongly on the BCR-antigen binding affinity when the antigen is associated with non-internalizable surfaces, compared to antigen bound to particles that can be internalized (Batista and Neuberger 2000). Recent studies using antigen-coated beads, planar lipid bilayers, or plasma membrane (PM) sheets revealed two major mechanisms by which B-cells extract antigen from non-internalizable surfaces for endocytosis. Mechanical forces, generated by non-muscle myosin II (NMII) activation at sites of antigen-BCR interaction, can directly pull antigen from presenting surfaces for endocytosis. When mechanical forces alone are not sufficient, hydrolases released from lysosomes cleave surface-associated antigen to facilitate internalization (Yuseff *et al.* 2011; Natkanski *et al.* 2013; Spillane and Tolar 2017; J. Wang *et al.* 2018). Surface-associated antigen was previously shown to induce polarization of B-cell lysosomes towards antigen-binding sites (Yuseff *et al.* 2011), but the mechanism responsible for triggering lysosome exocytosis and release of hydrolytic enzymes was unknown.

When cells are permeabilized by physical tearing or by pore-forming proteins, Ca^{2+} influx triggers rapid exocytosis of lysosomes as part of the process that repairs the PM and prevents cell death (Reddy *et al.* 2001; Andrews *et al.* 2014). Since its discovery several decades ago (Rodríguez *et al.* 1997), Ca^{2+}-dependent exocytosis of lysosomes has been observed in many cell types (Zhang *et al.* 2007; Naegeli *et al.* 2017; Villeneuve *et al.* 2018; Ibata *et al.* 2019). We previously reported that permeabilizing the PM of mouse splenic B-cells with the pore-forming toxin streptolysin O (SLO) triggers lysosomal exocytosis, releasing hydrolases extracellularly and exposing the luminal epitope of the lysosome-associated protein LIMP-2 on the cell surface.

B-cells rapidly reseal these PM lesions, in a process that requires lysosomal exocytosis (Miller *et al.* 2015). Surprisingly, here we found that interaction of the BCR with surface-associated antigen can permeabilize the B-cell PM, triggering a resealing mechanism that involves exocytosis of lysosomes. We investigated this process by determining if antigen-induced PM permeabilization depends on BCR-antigen binding affinity, BCR signaling and NMII motor activity, and if it influences the ability of B-cells to internalize and present surface-associated antigens to T-cells.

Results

BCR interaction with surface-associated antigen induces B-cell PM permeabilization at antigen-binding sites

We initially utilized two experimental models previously used to study BCR-mediated internalization of surface-associated antigen: $F(ab')_2$-anti-mouse IgM+G (αM, which binds and activates mouse BCRs) immobilized on beads or tethered to planar lipid bilayers (PLB) by biotin-streptavidin interaction. Beads or PLB coated with transferrin (Tf) at similar surface density were used as controls, as Tf does not activate the BCR and interacts with the Tf receptor with similar affinity as binding of the *bona fide* antigen hen egg lysozyme (HEL) to the BCR of transgenic MD4 mouse B-cells (Batista and Neuberger 1998; Fuchs and Gessner 2002). Strikingly, live-cell imaging revealed entry of the membrane-impermeable dye propidium iodide (PI) at B-cell locations in contact with αM-beads, indicating that PM permeabilization occurred at bead-binding sites (*Figure 1A, Figure 1-figure supplement 1, and Videos 1-3*). While similar percentages of B-cells bound αM- or Tf-beads (*Figure 1B),* a significantly higher fraction of B-cells binding αM-beads became PI-positive (*Figure 1C*). Flow cytometry analysis confirmed the

Figure 1

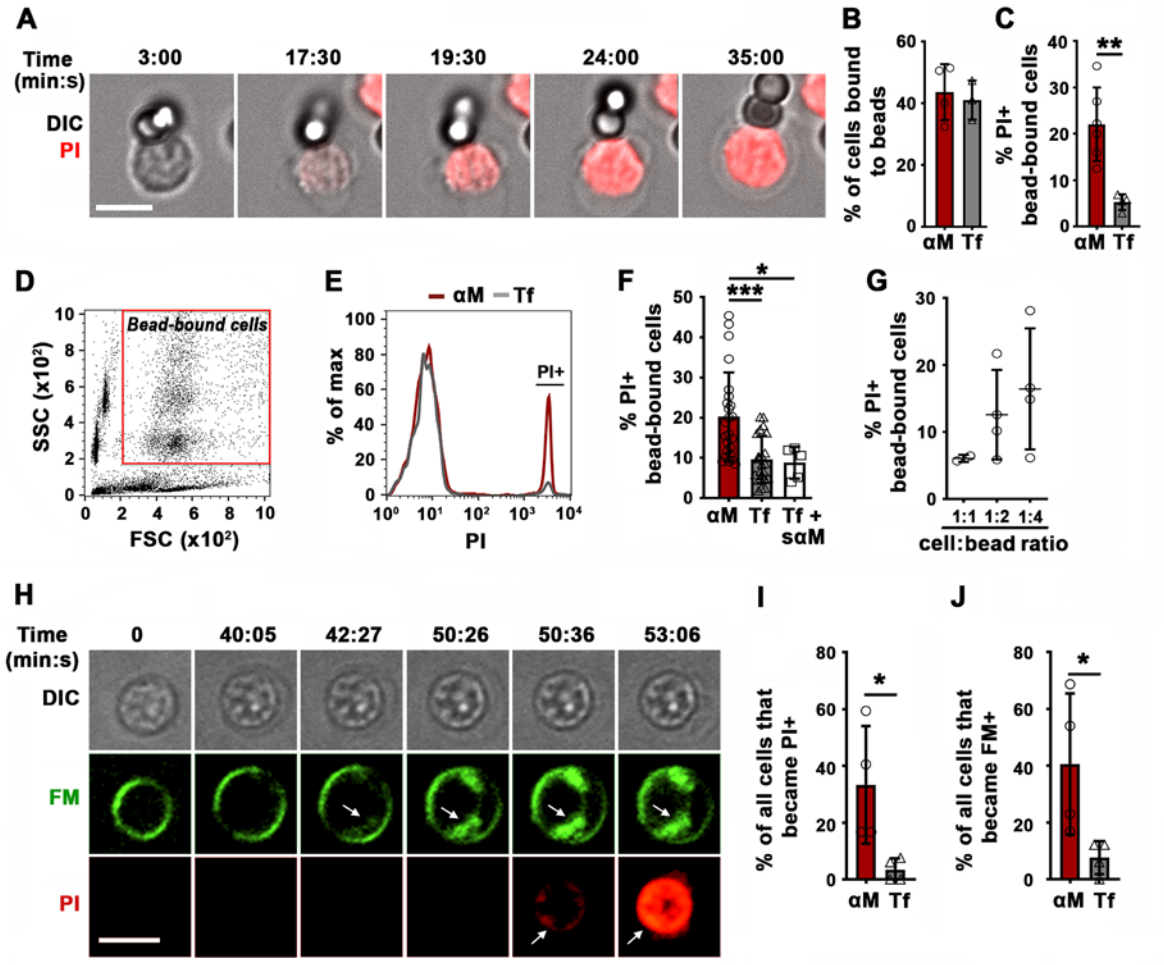

106

Figure 1. BCR binding to surface-associated ligands causes B-cell PM permeabilization. (**A**) Spinning disk time-lapse images of a splenic B-cell incubated with αM-beads (1:2 cell:bead ratio) in the presence of PI *(Video 1)*. (**B**) Percentages of B-cells bound to beads. Data points represent independent experiments (mean ± SD). (**C**) Percentages of PI-positive (PI+) cells in bead-bound B-cells at 30 min quantified from the images. Data points represent independent experiments (mean ± SD). (**D**) Gate for bead-bound B-cells in a flow cytometry forward and side scatter dot plot. (**E**) Histograms of PI fluorescence intensity (FI) of αM- and Tf-bead-bound B-cells after 30 min incubation. (**F**) Percentages of PI+ bead-bound B-cells after 30 min incubation with αM- or Tf-beads in the presence or absence of soluble αM (sαM). Data points represent independent experiments (mean ± SD). (**G**) Percentages of PI+ bead-bound B-cells after 30 min with αM-beads at indicated cell:bead ratios. Data points represent independent experiments (mean ± SD). (**H**) Spinning disk time-lapse images of a B-cell interacting with αM-PLB in the presence of FM1-43 and PI (arrows, FM1-43 or PI entry, *Video 4*). (**I**) Percentages of PI+ B-cells interacting with αM- or Tf-PLB for 30 min. Data points represent independent experiments (mean ± SD). (**J**) Percentages of B-cells interacting with αM- or Tf-PLB for 30 min and exhibiting intracellular FM staining (FM+). Data points represent independent experiments (mean ± SD). Bars, 5 μm. *$p \leq 0.05$, **$p \leq 0.01$, ***$p \leq 0.005$, unpaired Student's *t*-test or one-way ANOVA.

Figure supplement 1. BCR binding to αM-beads causes localized PM permeabilization in B-cells.

Figure supplement 2. Identification of bead-bound B-cells by flow cytometry.

Figure supplement 3. BCR binding to αM-beads does not increase apoptosis in B-cells.

Figure supplement 4. Sudden increases in intracellular FM staining in B-cells permeabilized during interaction with αM-PLB.

Figure supplement 5. The lipophilic FM dye enters B-cells permeabilized by αM-PLB, staining the nuclear envelope.

increased PI entry in B-cells binding αM-beads when compared to Tf-beads (*Figure 1D-G and Figure 1-figure supplement 2*). Addition of soluble F(ab')$_2$-anti-mouse IgM+G (sαM, also capable of binding and activating the BCR) did not increase the frequency of PI entry in B-cells binding to Tf-beads (*Figure 1F*). The percentage of cells positive for cleaved caspase-3, an early apoptotic marker, was similar in B-cells interacting or not with αM- or Tf-beads and only increased significantly after treatment with staurosporine (*Figure 1-figure supplement 3*), suggesting that PM permeabilization is not associated with apoptosis. Similar observations were made using the PLB system that allows lateral movement of the tethered antigen (Dustin *et al.* 2007). Significantly more B-cells became PI-positive when contacting αM-PLB when compared to Tf-PLB (*Figure 1H and I*).

PM permeabilization in B-cells binding to αM-PLB was also observed using membrane-impermeable lipophilic FM probes. These fluorescent dyes have been used extensively to assess PM integrity, because they only label the outer PM leaflet of intact cells but rapidly stain intracellular membranes when entering the cytosol (Bansal *et al.* 2003; McNeil *et al.* 2003; Demonbreun *et al.* 2019). After >30 min of interaction with αM-PLB, we observed sudden, massive increases in FM staining of intracellular membranes, including the nuclear envelope (*Figure 1H, arrows, Figure 1-figure supplements 4 and 5, and Video 4*). Consistent with the PI entry results (*Figure 1H and I)*, significantly more B-cells showed a sudden increase in intracellular FM staining when contacting αM-PLB when compared to Tf-PLB (*Figure 1H and J*). Sudden FM influx was only observed in B-cells that eventually became PI-positive, not in cells that remained PI-negative during interaction with αM-PLB. These observations, in addition to the minimal amounts of intracellular FM detected in all B-cells prior to 30-40 min, indicate

157 that the massive intracellular staining of B-cells binding αM-PLB reflects sudden PM
158 permeabilization and not gradual endocytosis of the dye.
159
160 As an independent method to demonstrate antigen-induced PM permeabilization in B-cells, we
161 took advantage of the ability of membrane-impermeable Ponceau 4R to quench cytosolic
162 fluorophores upon entering cells (Tay *et al.* 2019). Instead of monitoring nuclear or intracellular
163 membrane staining by membrane-impermeable fluorescent dyes, we determined the percentage
164 of B-cells pre-loaded with carboxyfluorescein succinimidyl ester (CFSE) that lost their cytosolic
165 fluorescence as a consequence of Ponceau 4R entry during PM permeabilization. To validate this
166 method, we first permeabilized B-cells with the pore-forming toxin streptolysin O (SLO). In the
167 presence of Ponceau 4R, the percentage of B-cells with reduced fluorescence levels of CFSE
168 increased significantly after exposure to SLO (*Figure 2A and B*), mimicking what we previously
169 observed for PI entry in SLO-treated B-cells (Miller *et al.* 2015). Thus, quenching of
170 cytoplasmic CFSE by the membrane-impermeable Ponceau 4R is a potent indicator of PM
171 permeabilization. Using this method, we compared B-cells incubated with αM- or Tf-PLB using
172 live-cell imaging. We found that a significantly higher percentage of CFSE-labeled B-cells
173 showed fluorescence quenching when interacting with αM-PLB, when compared to Tf-PLB
174 (*Figure 2C and D, and Video 5*). The average time for detection of αM-PLB-induced B-cell
175 permeabilization measured by this quenching method was similar to what was observed for FM
176 entry, while the average time for PI detection showed a ~8 min delay (*Figure 2E, Figure 1-figure*
177 *supplements 4, and Video 4*). Thus, FM influx and Ponceau 4R-mediated quenching are more
178 sensitive methods for detecting the onset of B-cell PM permeabilization when compared to PI
179 influx, which is only clearly visualized after intercalation into double-stranded DNA inside the

Figure 2

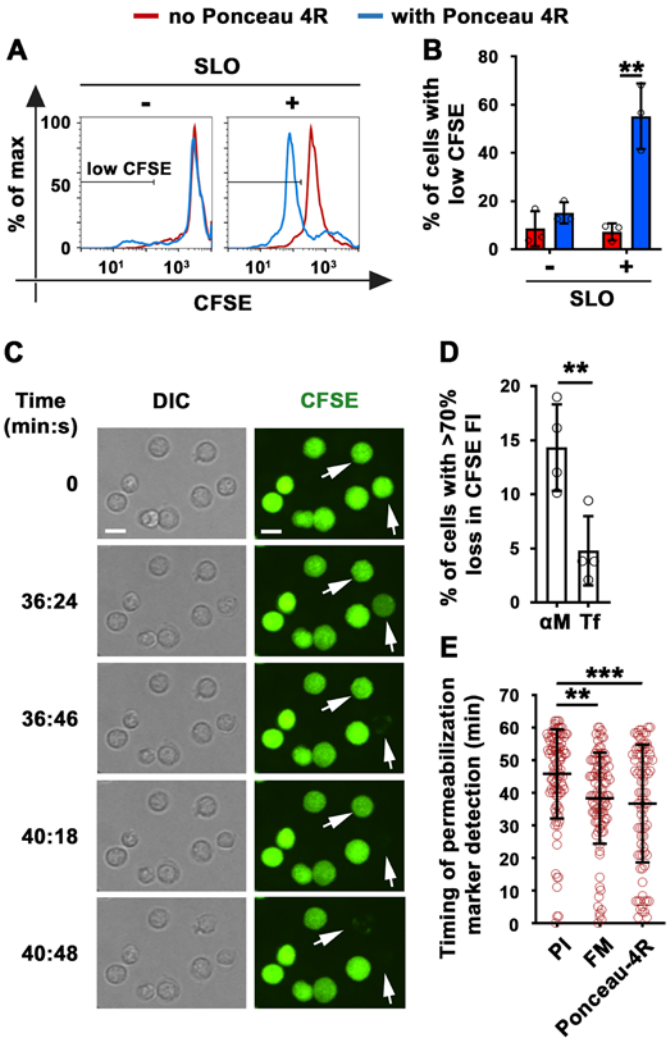

Figure 2. Extracellular Ponceau 4R quenches cytoplasmic CFSE in αM-PLB-permeabilized B-cells. (A) Histograms of CFSE FI in B-cells treated with or without SLO for 10 min in the presence or absence of Ponceau 4R by flow cytometry**. (B)** Percentages of cells with reduced CFSE in the presence or absence of Ponceau 4R, after treatment with or without SLO. Data points represent independent experiments (mean ± SD). **(C)** Spinning disk time-lapse images of B-cells pre-stained with CFSE interacting with αM-PLB in the presence of Ponceau 4R (arrows, cells showing Ponceau 4R quenching of cytoplasmic CFSE) *(Video 5)*. **(D)** Percentages of B-cells with more than 70% loss of CFSE FI after 60 min of interaction with αM- or Tf -PLB. Data points represent independent experiments (mean ± SD). **(E)** Timing of PI or FM1-43 entry or Ponceau 4R-mediated CFSE quenching in B-cells interacting with αM-PLB. Data points represent individual cells in at least four independent experiments (mean ± SD). Bars, 5 μm. $^{**}p \leq 0.01$, $^{***}p \leq 0.005$, unpaired Student's *t*-test or one-way ANOVA.

194 nucleus. Thus, based on consistent results obtained with three different methods, we conclude
195 that BCR binding to αM-coated surfaces (but not to soluble αM) causes localized
196 permeabilization of the B-cell PM.
197
198 We next determined whether HEL, a *bona fide* antigen recognized by the BCR of B-cells from
199 MD4 mice, also caused B-cell permeabilization when tethered to artificial surfaces or presented
200 as an integral membrane protein (mHEL) (Batista *et al.* 2001) on the surface of live cells. Flow
201 cytometry analysis revealed that similar fractions of MD4 B-cells become PI-positive after
202 binding beads coupled to αM or to HEL (*Figure 3A-C*). In contrast, WT B-cells binding to HEL-
203 beads showed a low percentage of PI-positive cells, similar to what was observed with Tf-beads
204 (*Figure 1F and Figure 3A-C*). Importantly, MD4 B-cells interacting with live COS-7 cells
205 expressing surface-associated mHEL-GFP showed marked co-clustering of the BCR and mHEL-
206 GFP at cell-cell interaction sites, followed by PI influx. This pattern was not observed in WT B-
207 cells whose BCR is incapable of specifically recognizing HEL (*Figure 3D* and *Videos 6 and 7*).
208 A significantly higher percentage of MD4 B-cells showed PI influx after interaction with mHEL-
209 GFP-expressing COS-7 cells, when compared to WT B-cells (*Figure 3E*). The percentage of PI-
210 positive MD4 B-cells was also significantly higher after incubation with mHEL-expressing
211 COS-7 cells than with mock-transfected cells (*Figure 3F*). Collectively, these results show that
212 BCR binding to surface-associated antigen can cause localized permeabilization of the B-cell
213 PM.
214

Figure 3

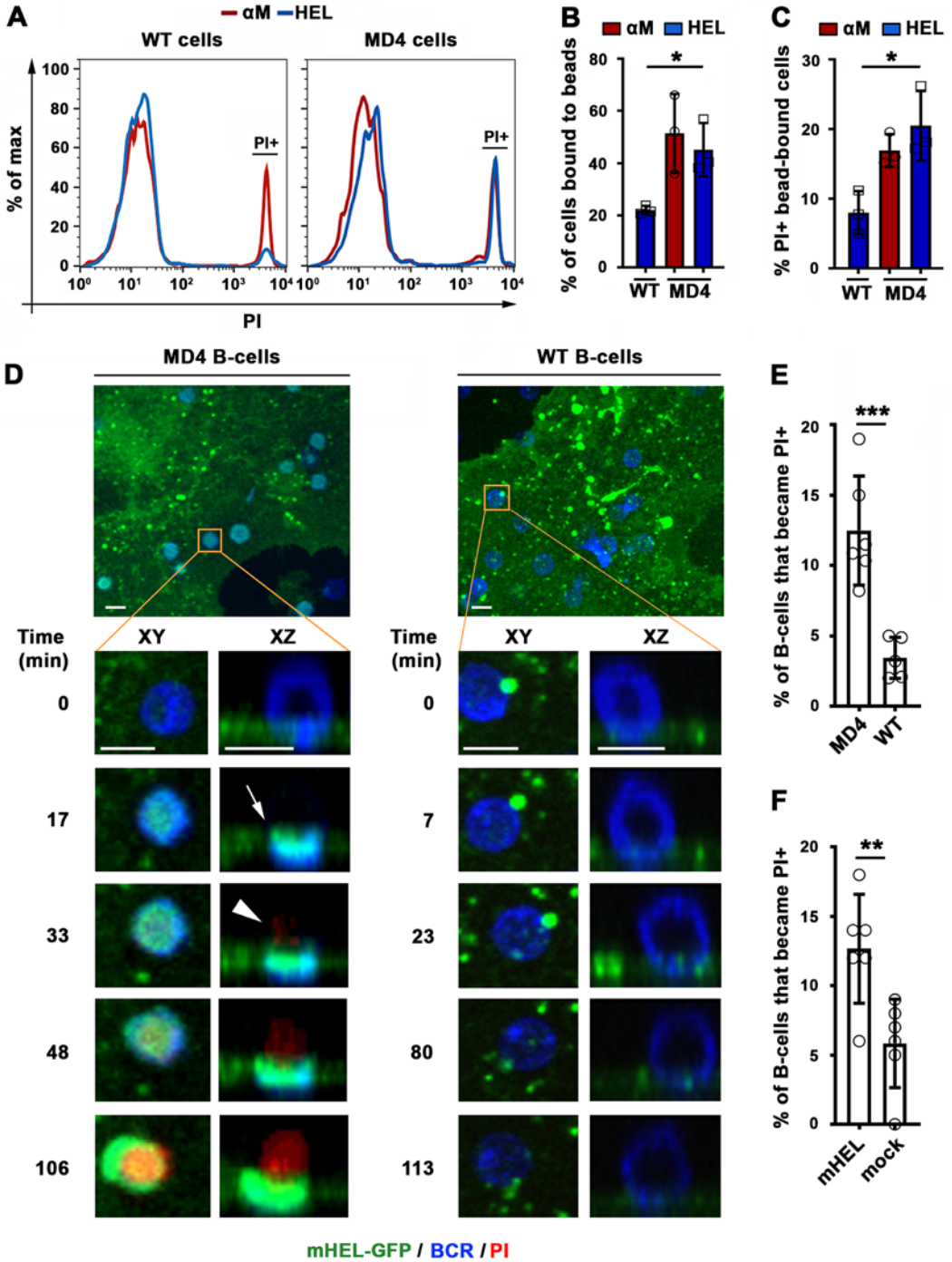

215

Figure 3. BCR-mediated binding of HEL coupled to beads or expressed as a transmembrane protein on COS-7 cells causes B-cell PM permeabilization. (A) Histograms of PI FI in WT or MD4 B-cells incubated with αM- or HEL-beads for 30 min by flow cytometry. (**B**) Percentages of WT and MD4 B-cells binding αM- or HEL-beads. Data points represent independent experiments (mean ± SD). (**C**) Percentages of PI+ bead-bound WT or MD4 B-cells after 30 min incubation. Data points represent independent experiments (mean ± SD). **(D)** Spinning disk time-lapse images of an MD4 B-cell (left panels) and a WT B-cell (right panels) interacting with a COS-7 cell expressing mHEL-GFP in the presence of PI *(Videos 6 and 7)*. Arrows, clustering of mHEL-GFP during B-cell binding; arrowheads, intracellular PI. **(E)** Percentages of PI+ MD4 and WT B-cells interacting with COS-7 cells transfected with mHEL-GFP. **(F)** Percentages of PI+ MD4 B-cells interacting with COS-7 cells transfected with mHEL-GFP or mock-transfected. Data points (E and F) represent individual videos from 3~4 independent experiments (mean ± SD). Bars, 5 μm *$p \leq 0.05$, **$p \leq 0.01$, ***$p \leq 0.005$, unpaired Student's *t*-test or one-way ANOVA.

Antigen-induced B-cell permeabilization requires high-affinity BCR-antigen binding, BCR signaling, and NMII motor activity

High-affinity binding of the BCR to antigen bound to non-internalizable surfaces induces high levels of BCR signaling, cytoskeleton reorganization, and antigen endocytosis (Batista and Neuberger 1998; Batista and Neuberger 2000; Fleire *et al.* 2006). To examine the impact of BCR binding affinity on antigen-induced PM permeabilization, we incubated MD4 B-cells with beads coated with equal densities of HEL or the duck egg lysozyme isoform DEL-I. The MD4 BCR binds DEL-I with >100 fold lower affinity than it binds HEL (Langley *et al.* 2017). As expected, the percentage of B-cells binding multiple beads was reduced when the BCR-antigen affinity decreased, but B-cells binding one single bead were detected for both HEL and DEL-I, and also Tf (*Figure 4-figure supplement 1*). In these single bead-bound populations, DEL-I-beads caused significantly less PI entry than HEL-beads (*Figure 4A*). Inhibition of signaling with the Src kinase inhibitor PP2 (Cheng *et al.* 2001) (iSrc) or the Bruton's Tyrosine Kinase inhibitor AVL-292 (Aalipour and Advani 2013) (iBTK) (*Figure 4B and C*) also reduced PI entry in cells binding HEL-beads (*Figure 4D*). After contact with αM-PLB or αM-beads but not Tf-PLB or Tf-beads, surface BCRs became polarized towards PLB- or bead-binding sites within ~10 min, a period markedly shorter than what is required for detection of PM permeabilization through FM influx (*Figure 4E-H, Figure 4-figure supplements 2 and 3, and Video 8*). Importantly, the activated form of the actin motor protein NMII, detected through its phosphorylated light chain (pMLC), accumulated along with the BCR at αM-bead-binding sites (*Figure 4G, Figure 4-figure supplement 3, and Video 9*). The fluorescence intensity ratios (FIR) of surface BCRs and pMLC were significantly higher in B-cells binding αM-beads than in cells binding Tf-beads (*Figure 4H*

Figure 4

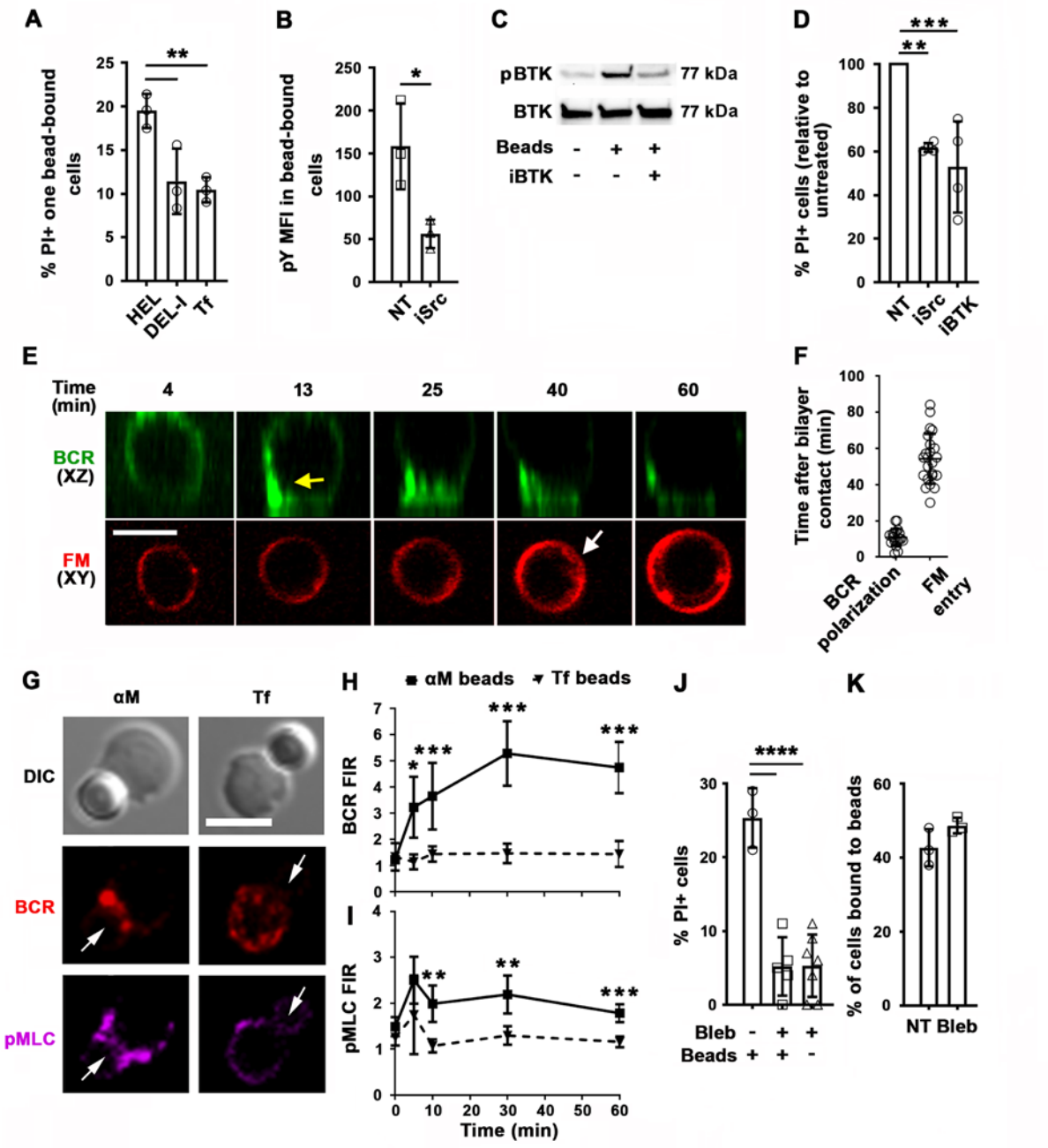

253

Figure 4. PM permeabilization induced by surface-associated antigen depends on high-affinity BCR-antigen binding, BCR signaling, and non-muscle myosin II (NMII) motor activity. (**A**) Percentages of PI+ single bead-binding B-cells after incubation with HEL-, DEL-I- or Tf-beads (1:4 cell:bead ratio) for 30 min. Data points represent independent experiments (mean ± SD). (**B**) Mean fluorescence intensity (MFI) of phosphotyrosine (pY) in HEL-bead-bound B-cells treated or untreated (NT) with a Src kinase inhibitor (iSrc) by flow cytometry. Data points represent independent experiments (mean ± SD). (**C***)* Western blot analysis of pBTK and BTK in B-cells incubated with HEL-beads in the presence or absence of a BTK inhibitor (iBTK) for 30 min. (**D**) Percentages of PI+ HEL-bead-bound cells treated with iSrc or iBTK relative to NT at 30 min. Data points represent independent experiments (mean ± SD). (**E**) Spinning disk time-lapse images of BCR polarization (yellow arrow) in a B-cell incubated with αM-PLB in the presence of FM4-64 (white arrow, intracellular FM). (**F**) Timing of BCR polarization and FM entry of individual cells interacting with αM-PLB *(Video 8)*. Data points represent individual cells in three independent experiments (mean ± SD). (**G**) Confocal images of BCR and phosphorylated NMII light chain (pMLC) staining in B-cells interacting with αM- or Tf-beads (arrows, bead binding sites). (**H** and **I**) Mean fluorescence intensity ratio (FIR) of BCR (**H**) and pMLC (**I**) staining at the bead-binding site relative to the opposite PM in αM- and Tf-bead-bound cells over time. Data represent the averages of three independent experiments (mean ± SD). (**J**) Percentages of PI+ bead-binding B-cells incubated with αM-beads for 30 min in the presence or absence of blebbistatin (Bleb). Data points represent individual videos from three independent experiments (mean ± SD). (**K**) Percentages of bead-bound B-cells incubated with αM-beads for 30 min in the presence or absence of Bleb. Data points represent independent experiments (mean ± SD). Bar, 5 μm. *$p \leq 0.05$, **$p \leq 0.01$, ***$p \leq 0.005$, ****$p \leq 0.001$, unpaired Student's *t*-test or one-way ANOVA.

Figure supplement 1. Impact of BCR-antigen affinity on B-cell-bead binding.

Figure supplement 2. B-cell binding to αM-PLB but not to Tf-PLB triggers BCR polarization first and PM permeabilization later.

Figure supplement 3. BCR and phosphorylated myosin light chain (pMLC) polarize towards αM-bead binding sites.

and I). Inhibition of NMII motor activity with blebbistatin (Bleb) markedly reduced the number of B-cells that became PI-positive during interaction with αM-beads, without affecting the cells' ability to bind the beads (*Figure 4J and K*). Live-imaging detected PI entry following a "tug-of-war' between two B-cells simultaneously engaging an αM-bead (*Video 3 and Figure 1-figure supplement 1C*), further supporting a role for NMII-mediated traction forces in antigen-induced PM permeabilization. Thus, our results indicate that PM permeabilization caused by surface-associated antigen requires strong BCR-antigen interaction and the subsequent activation of signaling and NMII motor activity.

Antigen-induced B-cell permeabilization triggers lysosome exocytosis as a repair response

B-cell permeabilization with the pore-forming toxin SLO triggers lysosomal exocytosis (Miller *et al.* 2015), a response required for sealing PM wounds (Reddy *et al.* 2001). In this study, we found that B-cells permeabilized during interaction with surface-associated antigen also rapidly reseal their PM, by utilizing an assay involving sequential exposure to the membrane-impermeable dyes FM4-64 and SYTOX Blue. Repaired cells were quantified by flow cytometry as the percentage of permeabilized αM-bead-binding cells (stained intracellularly with FM4-64 kept throughout the assay) that excluded the membrane-impermeable dye SYTOX Blue (added only during the last 10 min of the assay) (*Figure 5A*). Inhibition of lysosomal exocytosis with bromoenol lactone (BEL) (Fensome-Green *et al.* 2007; Tam *et al.* 2010) significantly reduced the percentage of resealed cells (*Figure 5A and B*) while not increasing the numbers of dead cells (*Figure 5-figure supplement 1*). These data suggest that lysosomal exocytosis is required for the resealing of B-cells permeabilized by binding to surface-associated antigen.

Figure 5

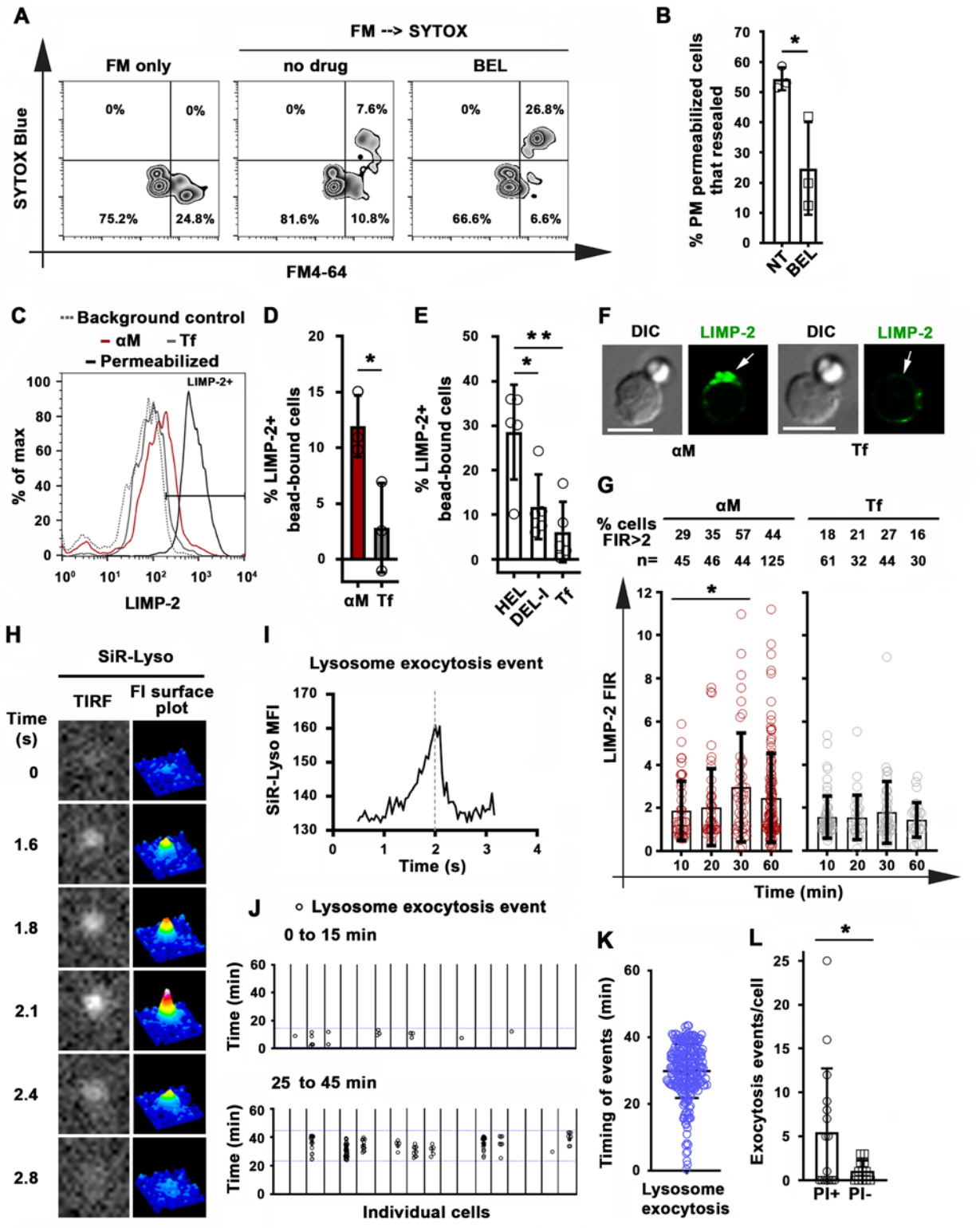

308

Figure 5. Antigen-induced permeabilization triggers PM repair mediated by lysosomal exocytosis. (**A**) Resealed bead-bound B-cells after incubation with αM-beads were assessed by flow cytometry analysis of FM4-64 (added at the start) and SYTOX Blue (added in the last 10 min) FI in the presence or absence of BEL. (**B**) Percentages of permeabilized αM-bead-bound cells that resealed in the presence or absence of BEL. Data points represent independent experiments (mean ± SD). (**C**) Flow cytometry analysis of surface-exposed (no detergent permeabilization) and/or intracellular LIMP-2 (with detergent permeabilization) of bead-bound B-cells after incubation with αM- or Tf-beads for 30 min. (**D** and **E**) Percentages of surface-exposed LIMP-2 (relative to values obtained with secondary antibody alone) in bead-bound B-cells incubated with αM- or Tf-beads (**D**) or with HEL-, DEL-I- or Tf-beads for 30 min (**E**). Data points represent independent experiments (mean ± SD). (**F**) Confocal images of surface-exposed LIMP-2 in B-cells incubated with αM- or Tf-beads (arrows, bead-binding sites). Bars, 5 μm. (**G**) FIR (bead-binding site: opposite PM) of surface-exposed LIMP-2 in individual cells over time. Data points represent individual cells (mean ± SD). (**H**) Total internal reflection microscopy (TIRF) images (left column) and FI surface plots (right column) of SiR-Lyso at the B-cell surface contacting αM-PLB (*Video 10*). (**I**) Representative MFI versus time plot of a SiR-Lyso-loaded lysosome undergoing exocytosis. (**J**) SiR-Lyso exocytosis events (circles) in individual B-cells during the first 0-15 min or 25–45 min of incubation with αM-PLB. (**K**) Times of individual SiR-Lyso exocytosis events in B-cells incubated with αM-PLB during a 45 min incubation. Data points represent individual SiR-Lyso exocytosis events from three independent experiments (mean ± SD). (**L**) Numbers of SiR-Lyso exocytosis events per B-cell permeabilized (PI+) or not permeabilized (PI-) by αM-PLB during a 45 min incubation. Data points represent individual cells from three independent experiments (mean ± SD). *$p \leq 0.05$, **$p \leq 0.01$, unpaired Student's *t*-test or one-way ANOVA.

Figure supplement 1. Bromoenol lactone (BEL) does not affect B-cell viability.

Figure supplement 2. BCR-mediated binding of αM-beads induces surface exposure of the LIMP-2 luminal domain at bead contact sites.

Figure supplement 3. Detection of lysosomal exocytosis by total internal reflection fluorescence (TIRF) microscopy.

To determine if permeabilization by surface-associated αM or HEL triggers exocytosis of lysosomes in B-cells, we first examined the surface exposure of luminal epitopes of the lysosomal membrane protein LIMP-2. Flow cytometry analysis detected surface LIMP-2 in a higher percentage of B-cells binding αM-beads than in B-cells binding Tf-beads (*Figure 5C and D*). Notably, surface exposure of LIMP-2 was lower in MD4 B-cells binding DEL-I-beads compared to HEL-beads (*Figure 5E*). These results reveal a close correlation between the extent of PM permeabilization (*Figure 4A*) and lysosomal exocytosis induced by surface-associated αM, HEL or DEL-I (*Figure 5D-E*). Surface LIMP-2 was predominantly detected at sites of αM-bead binding (*Figure 5F and Figure 5-figure supplement 2*) and this polarized pattern, measured by FIR, increased after ~30 min of interaction with αM- but not Tf-beads (*Figure 5G*). Notably, this timeframe was similar to the period required for PM permeabilization (*Figure 2E*). Next, we performed live total internal reflection fluorescence (TIRF) microscopy of B-cells preloaded with the luminal lysosomal probe SiR-Lyso (a membrane-permeable fluorescent peptide that binds the lysosomal enzyme cathepsin D) while contacting αM-PLB. Exocytosis events were identified by rises in the fluorescence intensity of SiR-Lyso puncta (reflecting lysosome entry into the TIRF evanescent field adjacent to the PM) followed by sharp decreases within ~2 s (reflecting dye dispersion upon fusion of lysosomes with the PM) (*Figure 5H and I, Figure 5-figure supplement 3, and Video 10*). Exocytosis events were observed in the majority of individual PI-positive cells interacting with αM-PLB (*Figure 5J*) and occurred predominantly ~30-45 min after αM-PLB contact (*Figure 5J and K*), a timing similar to PM permeabilization and LIMP-2 exposure. Importantly, lysosomal exocytosis events were significantly more frequent in permeabilized B-cells when compared to B-cells that remained intact (*Figure 5L*).

Thus, permeabilization of B-cells by surface-associated antigen triggers localized lysosomal exocytosis at antigen-BCR interaction sites as a PM repair response.

B-cell permeabilization and lysosomal exocytosis facilitate internalization and presentation of surface-associated antigen

We investigated the relationship between PM permeabilization by surface-associated antigen and antigen internalization using fluorescent αM covalently bound to beads or tethered to PLB. Live-cell imaging detected αM puncta moving away from bead-binding sites into B-cells, increasing progressively between 30 and 60 min of interaction (*Figure 6A and B and Video 11*). In contrast, intracellular fluorescent puncta were markedly less abundant during the same time period in cells not binding αM-beads, or binding Tf-beads (*Figure 6B*). Inhibition of antigen-mediated PM permeabilization with blebbistatin significantly reduced the extraction and internalization of αM coupled to beads (*Figure 6C*). When similar experiments were performed with PLB, the fraction of cells containing internalized αM and the total amount of αM uptake were significantly higher in permeabilized cells with high levels of intracellular FM staining (FM-high), compared to non-permeabilized cells with low intracellular FM staining (FM-low) (*Figure 6D-F*). Collectively, these data suggest that αM-induced PM permeabilization, rapidly followed by lysosomal exocytosis, promotes extraction and internalization of αM from non-internalizable surfaces.

Next, we investigated whether antigen internalization enhanced by PM permeabilization and lysosomal exocytosis impacts antigen presentation by B-cells. We compared levels of IL-2 secretion by the 3A9 T-cell hybridoma line (Allen and Unanue 1984) after activation by B-cells

Figure 6

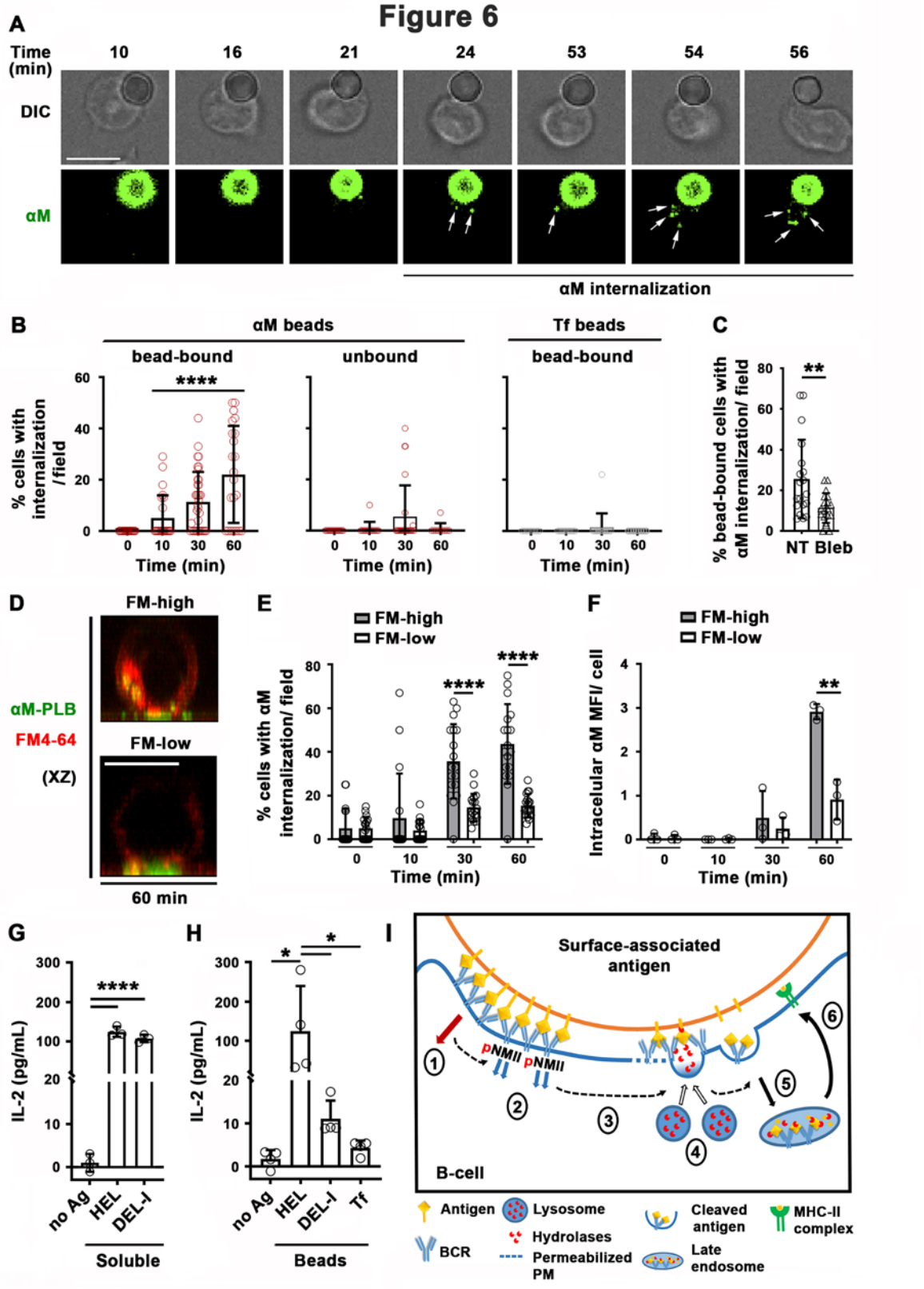

384

Figure 6. Antigen-induced PM permeabilization promotes antigen internalization and presentation. (**A**) Confocal live imaging of a B-cell interacting with fluorescent αM-beads (arrows, internalized αM). (**B**) Percentages of cells containing internalized αM or Tf, bound or not to αM- or Tf-beads, over time. Data points represent individual fields in three independent experiments (mean ± SD). (**C**) Percentages of bead-bound B-cells with internalized αM in the presence or absence of Bleb after 60 min incubation. Data points represent individual fields in three independent experiments (mean ±SD). (**D**) Confocal images (xz) of αM internalization in B-cells permeabilized (FM-high) or not permeabilized (FM-low) by αM-PLB after 60 min incubation. (**E**) Percentages of B-cells, permeabilized (FM-high) or not permeabilized (FM-low) by αM-PLB, containing internalized αM over time. Data points represent individual fields in three independent experiments (mean ± SD). (**F**) Average values of the mean fluorescence intensity (MFI) of internalized αM in individual B-cells permeabilized (FM-high) or not permeabilized (FM-low) by αM-PLB over time. Data points represent independent experiments (mean ± SD). (**G**) IL-2 secretion by 3A9 T-cells activated by B-cells incubated with or without (no Ag) soluble HEL or DEL-I (10 μg/ml) for 72 h. Data points represent independent experiments (mean ± SD). (**H**) IL-2 secretion by 3A9 T-cells activated by B-cells incubated with or without HEL-, DEL-I- or Tf-beads (1:4 cell:bead ratio) for 72 h. Bar, 5 μm. Data points represent independent experiments (mean ± SD). *$p \leq 0.05$, **$p \leq 0.01$, ****$p \leq 0.0001$, unpaired Student's *t*-test or one-way ANOVA. (**I**) Cartoon depicting a working model for the spatiotemporal relationship of events initiated by the interaction of the BCR with surface-associated antigen. High-affinity binding stabilizes BCR-antigen bonds and induces strong BCR signaling (1) and NMII activation (2). Activated NMII generates local traction forces that permeabilize the PM (3), which triggers a localized PM repair response mediated by lysosomal exocytosis. Lysosome exocytosis releases hydrolases that can cleave antigen off surfaces (4), facilitating endocytosis (5) and presentation to T-cells (6).

exposed to HEL- or DEL-I-beads. B-cells exposed to high concentrations of soluble HEL or DEL-I induced similar levels of IL-2 secretion (*Figure 6G*), demonstrating that the primary B-cells used in these assays could process and present the conserved peptide present in both HEL and DEL-I for T-cell activation. In contrast, when the B-cells were exposed to lower amounts of surface-associated antigens, B-cells exposed to HEL-beads activated T-cells to produce IL-2 at markedly higher levels than cells exposed to DEL-I-beads *(Figure 6H*). These results indicate that B-cell permeabilization resulting from high-affinity antigen-BCR interaction, with its corresponding lysosomal exocytosis response, facilitates the presentation of antigen associated with non-internalizable surfaces.

Discussion

Extracellular release of lysosomal enzymes by B-cells was previously proposed to cleave antigens tightly associated with non-internalizable surfaces, facilitating their internalization and presentation to T-cells (Yuseff *et al.* 2011; Spillane and Tolar 2017). However, it was unclear which mechanism was responsible for inducing lysosomal enzyme release when B-cells engaged insoluble antigen. In this study, we show that interaction of the BCR with surface-associated antigen can permeabilize the B-cell PM, triggering lysosomal exocytosis as part of the PM repair response (Rodríguez *et al.* 1997; Reddy *et al.* 2001). Antigen-dependent PM permeabilization occurs at antigen-binding sites, and is reversible under conditions that allow lysosomal exocytosis. We further demonstrate that PM permeabilization and lysosomal exocytosis require high-affinity binding of the BCR to antigen, BCR signaling, and activation of NMII motor activity, and that this process facilitates antigen internalization, processing and presentation. Thus, our study identifies a critical novel step in the affinity-dependent process by which B-cells

capture antigen tightly associated with surfaces, for effective internalization and subsequent presentation to T-cells.

Capture and internalization of antigen tightly associated with surfaces is an immunologically important process, as B-cells encounter this type of antigen *in vivo* on parasites, bacteria and viruses, as well as immune cells such as follicular dendritic cells. Follicular dendritic cells capture antigen drained into lymph nodes and present it on their surface to germinal center B-cells. In this manner, follicular dendritic cells enhance BCR antigenic stimulation by increasing antigen avidity, in addition to providing costimulatory molecules (Natarajan *et al.* 2001). While the exact percentage is unknown, studies have suggested that the majority of antigens that B-cells encounter *in vivo* are in a membrane-associated form (Batista and Harwood 2009). Importantly, the capture, internalization, and presentation of such surface-associated antigens to T-cells play a critical role in selecting specific B-cells for survival, clonal expansion, and differentiation into long-lived high-affinity memory B-cells and antibody-secreting cells (Gitlin *et al.* 2014).

We found that B-cell PM permeabilization induced by surface-associated antigen depends on the motor activity of NMII. Following BCR polarization, activated NMII accumulates at sites of B-cell binding to αM- or HEL-beads or PLB before PM permeabilization occurs. These findings are consistent with previous studies showing that internalization of surface-associated but not soluble antigen requires NMII-mediated traction forces at antigen-binding sites (Natkanski *et al.* 2013; Spillane and Tolar 2018). Collectively, our results support the notion that NMII-mediated traction forces generated during BCR-antigen interaction are responsible for permeabilization of

456 the B-cell PM. Whether this permeabilization is due to tearing of the lipid bilayer (Andrews *et al.*
457 2014) or the opening of mechanosensitive membrane channels (Liu *et al.* 2018; Liu and Ganguly
458 2019) is currently unknown. However, B-cell resealing was inhibited when lysosomal
459 exocytosis, a component of the PM repair response, was blocked (Reddy *et al.* 2001).
460 Furthermore, Endophilin A2, a protein that facilitates PM repair (Corrotte *et al.* 2020), also
461 contributes to BCR-mediated internalization of membrane-associated antigen (Malinova *et al.*
462 2020). Finally, three different membrane-impermeable probes, PI, FM lipophilic dyes, and
463 Ponceau 4R, gained access to the cytosol after B-cell interaction with surface-associated antigen.
464 These results together strongly suggest that NMII-mediated membrane tearing is the mechanism
465 underlying antigen-dependent B-cell PM permeabilization.
466
467 We were initially surprised to detect B-cell PM permeabilization during BCR-mediated binding
468 of antigen tightly associated to surfaces, a process known to generate myosin-mediated forces as
469 a mechanism to capture antigen. To confirm that such an event does occur, we utilized three
470 different methods to detect PM permeabilization, two types of antigen, and three types of
471 presenting surfaces. All generated similar results. We first detected B-cell permeabilization
472 during interaction with surface-associated antigen by following the entry of membrane-
473 impermeable DNA-binding or lipophilic dyes. While these compounds bind to different
474 intracellular structures, both showed sudden rather than gradual increases in intracellular
475 staining, consistent with PM permeabilization and not dye endocytosis. To strengthen these
476 results, we designed an independent assay based on the ability of Ponceau 4R to enter B-cells
477 and quench the fluorescence of CFSE, a widely used live-cell dye that covalently labels cytosolic
478 molecules without affecting cell viability. Ponceau 4R has been used to reduce the extracellular

479 background of fluorescence-based assays because it is membrane-impermeable and potently
480 quenches the emission of fluorophores in the 490-560 nm range (Tay *et al.* 2019). We found that
481 Ponceau 4R influx rapidly quenches the fluorescence of CFSE-labeled B-cells, providing us with
482 an independent and accurate tool to determine the kinetics of antigen-induced PM
483 permeabilization. We also found that two different model antigens, αM and HEL (pseudo and
484 *bona fide*, respectively), can induce B-cell PM permeabilization when attached to surfaces. This
485 shows that BCR binding through *bona fide* antigen-binding sites is not a requirement for
486 generation of the mechanical forces leading to B-cell PM permeabilization. Finally, since
487 stiffness of the antigen-presenting surface appears to impact BCR signaling and antigen capture
488 (Spillane and Tolar 2017; J. Wang *et al.* 2018), it could be argued that antigen tethered to latex
489 beads or PLB assembled on glass coverslips represent unnaturally stiff surfaces that might cause
490 B-cell permeabilization. To investigate this issue, we utilized COS-7 cells expressing mHEL, a
491 surface-associated antigen previously shown to engage MD4 B cells *in vivo* when expressed in
492 mouse models (Hartley *et al.* 1991). Our finding that BCR engagement of mHEL on the surface
493 of COS-7 cells also induces PM permeabilization supports the notion that this process occurs
494 under physiological conditions and is likely to be relevant *in vivo*.
495
496 Not all B-cells binding surface-associated antigen were permeabilized, possibly due to the
497 heterogeneity of the primary B-cell population used in our assays. Splenic B-cells are present at
498 different stages of peripheral maturation and differentiation (Sagaert and De Wolf-Peeters 2003;
499 Allman and Pillai 2008), thereby binding antigen with variable affinities at different times, and
500 generating distinct responses. It will be interesting to examine further which subsets of B-cells

are more effective in capturing and presenting surface-associated antigen through NMII-dependent PM permeabilization.

The rapid exocytosis of lysosomes triggered by B-cell permeabilization uncovered in our study provides a mechanistic explanation for the previously reported affinity-dependent extraction and presentation of antigen associated with non-internalizable surfaces (Batista and Neuberger 2000). We showed that the low affinity DEL-I induces markedly lower levels of PM permeabilization, lysosome exocytosis, and antigen presentation than the high affinity HEL, when the two antigens are displayed on surfaces at similar densities. Surface association significantly enhances the avidity of antigens by increasing their valency, a process that can reduce the impact of BCR-binding affinity on BCR signaling, antigen internalization, and presentation when compared to soluble forms of the same antigen. However, this avidity effect is primarily observed with antigen associated with surfaces that B-cells are able to internalize (Batista and Neuberger 2000), and it is known that B-cell subsets such as native follicular B-cells have very low phagocytic capacity (Vidard *et al.* 1996). We envision that when antigen is strongly associated with non-internalizable surfaces, low-affinity BCR-antigen interactions are disrupted before B-cells can extract antigen. In this scenario, high-affinity BCR interactions would be critical for sustaining antigen binding under NMII-mediated traction forces, to promote PM permeabilization, lysosomal enzyme release, and antigen extraction. High-affinity BCR-antigen binding is also expected to induce more robust signaling than low-affinity binding, enabling higher levels of NMII activation (Fleire *et al.* 2006; Natkanski *et al.* 2013) and polarization to drive PM permeabilization. Collectively, in addition to supporting the notion that tight antigen attachment to non-internalizable surfaces facilitates B-cell affinity discrimination, our results expand the

mechanistic understanding of why different physical and chemical forms (size, solubility, geometry, and molecular patterns) of immunogens impact the efficacy of vaccines (Bachmann and Jennings 2010; Khan *et al.* 2015).

Our study also provides important insight into the spatiotemporal relationship of events initiated by interaction of the BCR with surface-associated antigen (*Figure 6I*). Our results suggest that high-affinity binding stabilizes BCR-antigen bonds, inducing strong BCR signaling and NMII activation to locally generate traction forces that permeabilize the PM. Ca^{2+} entry then triggers a localized PM repair response mediated by lysosomal exocytosis, releasing hydrolases that can cleave antigen off surfaces, facilitating endocytosis and presentation to T-cells. Thus, our results support the notion that B-cells utilize a cellular mechanism that evolved for surviving PM injury to promote the acquisition, presentation, and possibly affinity discrimination of surface-associated antigens.

Materials and Methods

Key resources table

Reagent type (species) or resource	Designation	Source or reference	Identifiers	Additional information
Primary cell (spleen - C57BL/6)	WT	Jackson Laboratories	000664	
Primary cell (spleen - C57BL/6-Tg(IghelMD4)4Ccg/J)	MD4	Jackson Laboratories	002595	
Primary cell (spleen B10.BR-H2^{K2} H2-T18^{a}/ SgSnJJrep	B10.BR-H2^{K2} H2-T18^{a}/ SgSnJJrep	Jackson Laboratories	004804	
Cell line (*Mus musculus*)	A20	ATCC	TIB-208	B-cell lymphoma
Cell line (*Mus musculus*)	3A9	ATCC	CRL-3293	T-cell hybridoma

Cell line (*Cercopithecus aethiops*)	COS-7	ATCC	CRL-1651	Kidney fibroblasts
Reagent	Latex NH_2-beads	Polysciences	17145-5	
Ligand	αM ($F(ab')_2$ goat-anti-mouse IgM+G)	Jackson Immune Research	115-006-068	Binds to BCR
Antigen	HEL (Hen egg lysozyme)	Sigma-Aldrich	L6876	Binds to BCR from MD4 mice
Antigen	DEL-1 (Duck egg lysozyme)	David B. Langley and Daniel Christ laboratory		Binds to BCR from MD4 mice
Ligand	Tf (Holo- transferrin)	Sigma-Aldrich	T0665-50MG	Binds to transferrin receptor
Ligand	AF488-αM	Jackson Immune Research	115-546-003	Binds to BCR
Ligand	AF488-Tf	Thermo Fisher Scientifc	T13342	Binds to transferrin receptor
Commercial kit	BCA kit	Thermo Fisher Scientific	23235	Protein measurement during bead preparation
Control for antigen	Biotinylated transferrin (Tf-PLB)	Sigma-Aldrich	T3915-5MG	
Reagent	Streptavidin-conjugated Yellow-Green latex beads	Polyscience	24159-1	
Ligand	Biotin-SP (long spacer)-conjugated Fab fragments of goat-anti-mouse IgG (H+L)	Jackson Immune Research	115-067-003	
Inhibitor	Bleb (Blebbstatin)	Sigma-Aldrich	B0560	50 µM
Antibody	anti-phosphotyrosine mAb 4G10	Millipore	05-321	1:500
Antibody	AF488-goat-anti-mouse IgG_{2b}	Thermo Fisher Scientific	A-21141	
Reagent	PI (Propidium iodide)	Sigma-Aldrich	P4170-10MG	50 µg/ml
Reagent	FM1-43FX	Thermo Fisher Scientific	F35355	10 µg/ml

Reagent	FM4-64FX	Thermo Fisher Scientific	F34653	10 µg/ml
Reagent	SYTOX™ Blue nucleic acid stain	Invitrogen	S11348	300 nM
Inhibitor	Staurosporine	Abcam	120056	Apoptosis induction (1 µM)
Antibody	Cleaved Caspase-3 (Asp175) Antibody	Cell Signaling	9661T	1:500
Antibody	Cy5-Fab donkey-anti mouse IgG	Jackson ImmunoResearch	715-175-151	5 µg/ml
Antibody	Donkey anti-Rabbit IgG (H+L) Highly cross-adsorbed secondary antibody, Alexa Fluor 488	Thermo Fisher Scientific	A-21206	1:200
Inhibitor	PP2	Millipore-Sigma	529573	Src kinase inhibitor (5 µM)
Inhibitor	AVL-292	Selleckchem	S7173	BTK inhibitor (10 nM)
Antibody	anti-BTK	Cell Signaling	8547	1:1000
Antibody	Rabbit anti-phospho-BTK	Abcam	68217	1:500
Antibody	HRP goat-anti-rabbit	Jackson Immune Research	111-035-144	1:1000
Antibody	Cy3-Fab donkey-anti–mouse IgM+G	Jackson Immune Research	115-165-166	1:200
Antibody	Rabbit anti-phosphorylated myosin light chain (pMLC)	Cell Signaling	3671S	1:50
Antibody	AF633-goat-anti-rabbit IgG	Invitrogen	A-21070	1:500
Inhibitor	BEL (Bromoenol lactone)	Sigma-Aldrich	B1552	12 µM
Commercial kit	SiR-Lysosome and Verapamil	Cytoskeleton	CY-SC012	Lysosome probe 1 µM and 10 µM
Antibody	Rabbit-anti-LIMP-2	Sigma-Aldrich	SAB3500449-100UG	1:200
Antibody	AF488 donkey-anti-rabbit IgG	Life technology	A32790	1:200
Commercial kit	IL-2 ELISA kit	Biolegend	431804	
Software	FlowJo 10.1	FlowJo, LLC		https://www.flowjo.com/solutions/flowjo/downloads

Software	Volocity Suite	PerkinElmer		https://ir.perkinelmer.com/news-releases/news-release-details/perkinelmer-launches-volocityr-60-high-performance-3d-cellular
Software	NIH Image J			https://imagej.nih.gov/ij/
Software	MATLAB	MathWorks		https://www.mathworks.com/products/matlab.html
Software	Prism	GraphPad		https://www.graphpad.com/scientific-software/prism/
Antibody	Anti-CD90.2	Biolegend	105310	1 µl/ $2x10^6$ cells
Reagent	Guinea pig complement	Innovative Research	IGGPCSER	100 µl/ $4x10^7$ cells
Reagent	1,2-dioleoyl-sn-glycero-3-phosphocholine	Avanti Polar Lipids	850375P	5 mM (PLB)
Reagent	1,2-dioleoyl-sn-glycero-3-phosphoethanolamine-cap-biotin	Avanti Polar Lipids	870273C	50 µM (PLB)
Reagent	Ponceau 4R	Sigma-Aldrich	18137	1 mM
Reagent	CFSE	Thermo Fisher Scientific	C34553	1 µM
Reagent	Lipofectamine 3000	Thermo Fisher Scientific	L3000008	
Reagent	Bovine fibronectin	Millipore	341631	5 mg/ml

Mice, B-cell isolation and culture

Primary B-cells were isolated from the spleens of wild type C57BL/6, MD4 transgenic (C57BL/6 background), B10.BR-*H2*^{k2} *H2-T18*^{a}/SgSnJJrep (Jackson Laboratories), and F1 of B10.BR-*H2*^{k2} *H2-T18*^{a}/SgSnJJrep x MD4 mice using a previously published protocol (Miller *et al.* 2015). Briefly, mononuclear cells were isolated by Ficoll density-gradient centrifugation (Sigma-Aldrich). T-cells were removed with anti-mouse CD90.2 mAb (BD Biosciences) and guinea pig complement (Innovative Research, Inc.) and monocytes and dendritic cells by

548 panning. B-cells were kept at 37°C and 5% CO_2 before and during experiments. All procedures
549 involving mice were approved by the Institutional Animal Care and Usage Committee of the
550 University of Maryland.
551 The A20 B-cell lymphoma line (ATCC #TIB-208) was cultured in DMEM (Lonza)
552 supplemented with 10% of FBS (Thermo Fisher Scientific), 0.05 mM 2-mercaptoethanol
553 (Sigma-Aldrich), 10 mM MOPS, 100 units/ml penicillin, and 100 µg/ml streptomycin (Gemini)
554 at 37°C and 5% CO_2. The 3A9 T-cell hybridoma line (ATCC #CRL-3293) was cultured in
555 DMEM (ATCC) supplemented with 5% FBS (Thermo Fisher Scientific), 0.05 mM 2-
556 mercaptoethanol (Sigma-Aldrich) at 37°C and 5% CO_2.
557
558 **Antigen-coated beads**
559 Latex NH_2-beads (3 µm diameter, 3.5 x 10^8 beads/preparation, Polyscience) were activated with
560 8% glutaraldehyde in 0.5 ml PBS for 120 min under rotation at room temperature, washed with
561 PBS, and incubated overnight with equal molar amounts of F(ab')$_2$ goat-anti-mouse IgM+G
562 (αM, 20 µg/ml, Jackson ImmunoResearch Laboratories), hen egg lysozyme (HEL, 5.8 µg/ml,
563 Sigma-Aldrich), duck egg lysozyme (DEL)-I (Langley *et al.* 2017), holo-transferrin (Tf, 32
564 µg/ml, Sigma-Aldrich), Alexa Fluor (AF) 488-conjugated Tf (AF488-Tf, 32 µg/ml, Thermo
565 Fisher Scientific), or AF488-F(ab')$_2$ goat-anti-mouse IgM+G (AF488-αM, 20 µg/ml, Jackson
566 ImmunoResearch Laboratories) in 1 ml PBS. Protein content determination (BCA, Thermo
567 Fisher Scientific) of coupling solutions before and after bead incubation confirmed that similar
568 molar amounts of protein were conjugated in each case. The beads were then blocked with PBS
569 1% BSA in PBS for 30 min under rotation, washed to remove unconjugated proteins, counted in
570 a Neubauer chamber and stored at 4°C in PBS containing 1% BSA and 5% glycerol.

Streptavidin-conjugated Yellow-Green latex beads (2 μm diameter, 5 x 10^8 beads/preparation, Polyscience) were washed with 1% BSA in PBS and incubated with Biotin-SP (long spacer)-conjugated Fab fragments of goat-anti-mouse IgG (H+L) (40 μg of biotinylated antibody/mg of beads, Jackson ImmunoResearch Laboratories) for 30 min at 4°C, washed, counted in a Neubauer chamber and stored at 4°C in PBS containing 1% BSA and 5% glycerol.

Antigen-coated planar lipid bilayers (PLB)

PLB were prepared as previously described (Dustin *et al.* 2007; Liu *et al.* 2012; Spillane and Tolar 2017). Briefly, liposomes were generated from 5 mM 1,2-dioleoyl-sn-glycero-3-phosphocholine plus 1,2-dioleoyl-sn-glycero-3-phosphoethanolamine-cap-biotin (Avanti Polar Lipids) at a 100:1 molar ratio by sonication. Eight-well coverslip chambers (Lab-Tek) were incubated with liposomes for 20 min at room temperature and washed with PBS. The chambers were then incubated with 1 μg/ml streptavidin (Jackson ImmunoResearch Laboratories) for 10 min, washed, and incubated with 10 μg/ml mono-biotinylated Fab' goat-anti-IgM+G (αM-PLB) (Liu *et al.* 2012) or the same molar amount of biotinylated Tf (16 μg/ml, Sigma-Aldrich) (Tf-PLB) for 10 min at room temperature.

COS-7 cells expressing membrane hen egg lysozyme-GFP (mHEL-GFP)

COS-7 cells were transiently transfected with mHEL-GFP (Batista *et al.* 2001) (plasmid kindly provided by Dr. Michael Gold, University of British Columbia) using Lipofectamine 3000 (Thermo Fisher Scientific) and a published protocol (J.C. Wang *et al.* 2018), and used for experiments 24 h post-transfection.

Flow cytometry analysis of PM permeabilization

Mouse splenic B-cells were incubated with beads coated with αM, HEL, DEL-I or Tf in DMEM containing 6 mg/ml BSA (DMEM-BSA) at a cell:bead ratio of 1:2 (or as indicated), or with soluble $F(ab')_2$ goat-anti-mouse IgM+G (sαM, 0.5 μg/ml) for 30 min at 37°C with 5% CO_2. Propidium iodide (PI, Sigma-Aldrich) was present during the 37°C incubation as an indicator of PM permeabilization. Cells were then analyzed by flow cytometry (BD FACSCanto II) at 10,000 cell counts/sample. Bead-bound cells were identified based on their forward (FSC)- and side-scattering (SSC) properties and fluorescence intensity (FI) when using fluorescent beads (*Figure 1-figure supplement 2*). The percentages of PI-positive (PI+) cells among the bead-bound cell populations were quantified using FlowJo 10.1 software.

Live-cell imaging of PM permeabilization

To assess PM permeabilization by protein-coated beads, mouse splenic B-cells or a B-cell line (A20) were incubated for 30 min at 4°C in 35 mm glass-bottom dishes (MatTek) coated with poly-lysine and then with protein-coated beads at a cell to bead ratio of 1:2 for another 30 min at 4°C. Cells were washed with DMEM-BSA and imaged in a Live Cell System chamber (Pathology Devices) at 37°C with 5% CO_2 in the presence of 50 μg/ml PI (Sigma-Aldrich) with or without 50 μM blebbistatin (Sigma-Aldrich). Images were acquired for 60 min at 1 frame/15-30 s using a spinning disk confocal microscope (UltraVIEW VoX, PerkinElmer with a 63X 1.4 N.A. oil objective). Images were analyzed using Volocity Suite (PerkinElmer) and NIH ImageJ. More than 200 cells from 3 independent experiments were analyzed for each condition.

To analyze PM permeabilization by protein-coated PLB, splenic B-cells were incubated with FM1-43FX or FM4-64FX (Thermo Fisher Scientific) in DMEM-BSA for 5 min at 4°C,

added to coverslip chambers containing mono-biotinylated Fab' goat-anti-IgM+G or biotinylated Tf tethered to PLB, and imaged immediately at 37°C with 5% CO_2 in the presence of 50 μg/ml PI and/or 10 μg/ml FM1-43FX or FM4-64FX (Thermo Fisher Scientific) using a spinning disk confocal microscope (UltraVIEW VoX, PerkinElmer with a 63X 1.4 N.A. oil objective). Images were acquired at 1 frame/6-10 s and analyzed using Volocity (PerkinElmer) and NIH ImageJ. For quantitative analysis, the mean fluorescence intensity (MFI) of FM1-43FX or FM4-64FX in a defined area was measured using Volocity (PerkinElmer). More than 270 cells from 3 independent experiments were analyzed for each condition.

To analyze PM permeabilization by Ponceau 4R quenching, B-cells were pre-stained with 1 μM CFSE (Thermo Fisher Scientific) for 10 min at 37°C and washed with DMEM. Cells were then incubated with αM- or Tf -PLB and analyzed by a spinning disk confocal microscope (UltraVIEW VoX, PerkinElmer with a 40X 1.4 N.A. oil objective) in the presence or absence of 1 mM of Ponceau 4R (Sigma-Aldrich). More than 480 cells from 4 independent experiments were analyzed for each condition. To validate this method, cells pre-stained with CFSE were incubated with or without 800 ng/ml SLO in the presence or absence of 1 mM Ponceau 4R (Sigma-Aldrich) for 10 min and analyzed by flow cytometry (BD FACSCanto II) at 10,000 cell counts/sample.

To analyze PM permeabilization by antigen presented on the cell surface, COS-7 cells mock-transfected or transfected with mHEL-GFP were seeded onto fibronectin-coated coverslips and cultured for 24 h. WT or MD4 B-cells pre-stained with AF674-conjugated Fab fragments of donkey-anti–mouse IgM+G (Jackson ImmunoResearch Laboratories) were added to the COS-7 cell coverslips in the presence of 50 μg/ml PI and imaged immediately at 37°C and 5% CO_2 using a spinning disk confocal microscope (UltraVIEW VoX, PerkinElmer with a 40X 1.3 N.A.

oil objective). Images were acquired at 1 frame/20s and analyzed using NIH ImageJ software. More than 240 cells from 3 independent experiments were analyzed for each condition.

Cleaved caspase-3 detection

Splenic B-cells were pretreated or not with 1 µM staurosporine (Abcam) for 24 h at 37°C in DMEM-BSA to induce apoptosis (Diaz *et al.* 2004), exposed to αM- or Tf-beads for 30 min at 37°C, washed, fixed with 4% paraformaldehyde (PFA), blocked with 1% BSA, and permeabilized with 0.05% saponin. Cells were then incubated with antibodies specific for cleaved caspase-3 (Asp175) (Cell Signaling Technology) followed by AF488 donkey-anti-rabbit IgG (Life Technologies) and analyzed by flow cytometry (BD FACSCanto II) at 10,000 cell counts/sample. The percentages of cells with cleaved caspase-3 staining were determined using FlowJo 10.1 software.

BCR signaling

BCR signaling was analyzed using both flow cytometry and western blotting. For flow cytometry assays, splenic B-cells from MD4 mice were pretreated or not with 5 µM of the Src kinase inhibitor PP2 (Millipore) (Cheng *et al.* 2001) for 30 min at 37°C (conditions selected not to cause B-cell toxicity) and then incubated with HEL-beads in the presence or not of the inhibitor at 37°C for 30 min. Cells were fixed with 4% PFA, permeabilized with 0.05% saponin, incubated with mouse anti-phosphotyrosine mAb (4G10, Millipore) followed by AF488-goat-anti-mouse IgG_{2b} (Thermo Fisher Scientific) secondary antibodies, and analyzed by flow cytometry (BD FACSCanto II) at 10,000 cell counts/sample. The data were analyzed using FlowJo 10.1 software.

For western blot assays, splenic B-cells from MD4 mice were pretreated or not with 10 nM of the BTK inhibitor AVL-292 (Selleckchem) (Aalipour and Advani 2013) for 30 min at 37ºC (conditions selected not to cause B-cell toxicity) and incubated with HEL-beads in the presence or not of the inhibitor at 37°C for 30 min. Cells were then lysed using RIPA buffer (150 mM $NaCl_2$, 1% of NP40, 0.5% Sodium deoxycholate, 0.1% SDS, 50 mM Tris, pH 8.0) containing protease and phosphatase inhibitors (50 mM NaF, 1 mM Na_3VO_4 and 10 mM $Na_4P_2O_7$) at 4ºC. Cell lysates were run in 4-20% gradient SDS-PAGE gels (Bio-Rad) ($5x10^6$ cells/ lane) and transferred (Bio-Rad Trans-Blot transfer system) to PVDF membranes (Millipore). The membranes were blotted with rabbit anti-phospho-BTK (pBTK; Abcam) or anti-BTK (Cell Signaling Technology) followed by HRP-anti-rabbit antibodies (Jackson ImmunoResearch Laboratories) and visualization using ECL substrate (Bio-Rad) and imaging (iBright FL-1500, (Thermo Fisher Scientific).

To check if signaling affected PM permeabilization, splenic B-cells from MD4 mice were pretreated or not with 5 μM PP2 (Cheng *et al.* 2001) or 10 nM AVL-292 (Aalipour and Advani 2013) for 30 min at 37ºC and then incubated with HEL-beads in the presence or not of the inhibitor and 50 μg/ml PI (Sigma-Aldrich) at 37°C for 30 min. The percentage of PI+ cells was expressed relative to the untreated condition.

BCR and NMII polarization

BCRs on the surface of mouse splenic B-cells were stained with Cy3-Fab donkey-anti–mouse IgM+G (Jackson ImmunoResearch Laboratories) for 30 min at 4°C. Cells were then incubated with αM- or Tf-beads at 4°C for 30 min and 37°C for different lengths of time. Cells were fixed with 4% PFA, permeabilized with 0.05% saponin, and incubated with rabbit anti-phosphorylated

myosin light chain 2 (pMLC2) antibodies (Cell Signaling Technology) to label activated NMII (Bresnick 1999), followed by AF633-goat-anti-rabbit IgG (Invitrogen). Cells were analyzed by confocal fluorescence microscopy (Zeiss LSM710 with a 63X 1.4 N.A. oil objective). The percentages of cells with polarization of surface labeled BCRs and activated NMII towards bead-binding sites were quantified by visual inspection. More than 300 cells from 3 independent experiments were analyzed for each condition.

PM repair assay

Mouse splenic B-cells were pretreated or not with 12 μM bromoenol lactone (BEL, Sigma-Aldrich) in DMEM-BSA for 30 min at 37ºC before and during assays, to inhibit lysosomal exocytosis and PM repair (Fensome-Green *et al.* 2007). Cells were then incubated with αM-beads (1:2 cell-bead ratio) with or without inhibitors at 4ºC for 5 min and 37°C for 30 min in the presence of FM4-64FX (Thermo Fisher Scientific) to stain wounded cells. Cells were then incubated with SYTOX^{TM} Blue nucleic acid stain (300 nM, Invitrogen) at 4ºC for 10 min to stain cells that failed to repair PM wounds during the 30 min incubation. Cells were analyzed by flow cytometry (BD FACSCanto II) at 10,000 cell counts/sample. Cells that were FM4-64FX positive but SYTOX Blue negative were identified as permeabilized cells that resealed. The percentages of resealed cells among all bead-bound permeabilized cells were quantified using FlowJo 10.1 software.

BCR polarization in relation to permeabilization

Surface BCRs of splenic B-cells were labeled with Cy5-Fab donkey-anti mouse IgG (Jackson ImmunoResearch) at 4ºC for 30 min. Cells were incubated with αM-PLB in the presence of FM

4-64FX (Thermo Fisher Scientific) and imaged immediately at 37°C with 5% CO_2 using a confocal spinning disk confocal microscope (UltraVIEW VoX, PerkinElmer with a 60X 1.4 N.A. oil objective). Images were acquired at 1 frame/20 s for 60 min and analyzed using a custom-made MATLAB script (MathWorks) and NIH ImageJ software. BCR polarization was analyzed using maximal projection of XZ images and quantified by the MFI ratio between defined regions within the bottom half (closer to PLB) and the top half (away from PLB) of individual cells. Cells with bottom to top ratios ≥2 were considered polarized. More than 20 cells from 3 independent experiments were analyzed.

Lysosome exocytosis

To detect LIMP-2 exposed on the cell surface, splenic B-cells (C57BL/6 or MD4) were incubated with αM-, HEL-, DEL-I or Tf-beads for 30 min at 37°C, cooled to 4°C, and incubated with rabbit-anti-LIMP-2 antibodies (Sigma-Aldrich) for 60 min at 4°C. Cells were then washed and fixed with 4% PFA, washed, blocked with 1% BSA in PBS and incubated with AF488 donkey-anti-rabbit IgG (Life Technologies) secondary antibodies. For intracellular LIMP-2 staining, B-cells were fixed with 4% PFA, washed, permeabilized with 0.05% saponin for 20 min, and incubated with rabbit anti-LIMP-2 antibodies followed by AF488 donkey-anti-rabbit IgG. Flow cytometry (BD FACSCanto II) was performed at 10,000 cell counts/sample. Cells were also analyzed by confocal fluorescence microscopy (Leica SPX5 with a 63X 1.4 N.A. oil objective). Polarization of LIMP-2 towards bound beads was quantified by calculating the fluorescence intensity ratio (FIR) of anti-LIMP-2 at the B-cell-bead contact site relative to the opposite side of the cell PM, using NIH ImageJ and a custom-made MATLAB script (MathWorks).

732 Individual events of lysosome exocytosis were captured using total internal reflection
733 fluorescence (TIRF). Splenic B-cells were preloaded with SiR-Lysosome (1 µM, Cytoskeleton)
734 in the presence of verapamil (10 µM, Cytoskeleton) for 30 min at 37ºC. Cells were added to
735 coverslip chambers containing mono-biotinylated Fab' goat anti-IgM+G tethered to PLB and
736 imaged at 37°C with 5% CO_2 in the presence of PI (50 µg/ml, Sigma-Aldrich) using a TIRF
737 microscope (NIKON Eclipse Ti-E TIRF, 63X 1.49NA oil objective). Images were acquired at 8
738 frames/s during 15-20 min intervals of the 45 min incubation and analyzed using NIH ImageJ
739 and Nikon NIS Elements software. Increases in the FI of individual SiR-Lysosome puncta
740 (reflecting lysosome movement within the TIRF evanescent field towards the PM in contact with
741 PLB) followed by sharp decreases within a period of 1-2 s (corresponding to a loss of the SiR-
742 Lysosome signal upon PM fusion) were scored as exocytosis events (Jaiswal *et al.* 2004). More
743 than 20 cells were analyzed in 4 independent experiments.
744
745 **Antigen internalization**
746 For live-imaging of antigen internalization, splenic B-cells were incubated with AF488-αM-
747 beads (1:4 cell to bead ratio) in the presence of 1 µM SiR-Lysosome and 10 µM verapamil for 30
748 min at 4°C, washed with DMEM-BSA and imaged by confocal fluorescence microscopy (Leica
749 SPX5 with a 63X 1.4 N.A. oil objective) for 60 min at 1 frame/min at 37ºC. Live time-lapse
750 images were analyzed using NIH ImageJ.
751 For fixed cell imaging, splenic B-cells were pretreated or not with 50 µM blebbistatin on
752 poly-lysine coated slides for 30 min at 4°C and incubated with AF488-αM beads or AF488-Tf-
753 beads at 37°C for varying lengths of time in the presence or not of 50 µM blebbistatin. After
754 fixation with 4% PFA, cells were imaged by confocal fluorescence microscopy (Zeiss LSM710

with a 63X 1.4 N.A. oil objective). Percentages of cells with intracellularly-located AF488-αM puncta were determined by visual inspection of images. More than 200 cells from 3 independent experiments were analyzed for each condition.

For live-imaging of B-cells interacting with PLB, mouse splenic B-cells were added to coverslip chambers containing PLB coated with AF488-conjugated mono-biotinylated Fab' goat-anti-mouse IgM+G and incubated at 37°C with 5% CO_2 in the presence of 10 µg/ml FM 4-64FX (Thermo Fisher Scientific) for varying lengths of time. Samples were then moved to 4°C for 5 min and immediately imaged using a confocal microscope (Leica SPX5 with a 63X 1.4 N.A. oil objective). Internalization of antigen was quantified by determining the percentages of cells with intracellularly-located AF488-Fab' goat-anti-mouse IgM+G puncta in each field and by measuring the AF488 FI associated with intracellular puncta in individual cells, using a custom-made MATLAB (MathWorks) script. Cells with high FM staining were identified as wounded and those with low FM staining as unwounded. More than 15 fields or ~90 cells from 3 independent experiments (high or low FM staining) were analyzed for each condition.

Antigen presentation and T-cell activation

To detect antigen presentation to T-cells, splenic B-cells from F1 mice of a crossing between B10.BR-*H2*^{k2} *H2-T18*^{a}/SgSnJJrep and MD4 mice were co-cultured with 3A9 T-cell hybridoma cells (ATCC® CRL-3293™) at equal concentrations (3.5x10^6 cells/ml). Cells were incubated in DMEM supplemented with 5% FBS and 0.05 mM 2-mercaptoethanol for 72 h in the presence or not of soluble HEL or DEL-I (10 µg/ml), or of beads coated with HEL, DEL-I or Tf (1:4 cell to bead ratio). After incubation, the concentration of IL-2 in the supernatant was measured using an IL-2 ELISA kit (Biolegend).

778

779 **Statistical analysis**

780 Statistical significance was assessed using unpaired, two-tailed Student's *t*-tests (Prism -
781 GraphPad software) when only two groups were compared, and one-way ANOVA when 3 or
782 more groups were compared. All data were presented as the mean ± SD (standard deviation).

783

784 Acknowledgments

785 We thank Dr. A. Upadhyaya (Department of Physics, University of Maryland) for TIRF
786 microscopy equipment and advice, A. Beaven (CBMG Imaging Core, University of Maryland)
787 and K. Class (CBMG Flow Cytometry Core, University of Maryland) for assistance with
788 confocal microscopy and flow cytometry, Drs. S. K. Pierce and M. Akkaya (NIH) for the 3A9 T-
789 cell hybridoma, B. Mittra and J. Jensen (University of Maryland) for SLO expression and
790 purification, Dr. Michael Gold for providing the mHEL-GFP DNA construct, and members of
791 the Song and Andrews laboratories for helpful discussions. This work was supported by the NIH
792 grant R01 GM064625 to NWA and WS and NIH grant T32 GM080201 to JJHvH.

793

794 References

795 Aalipour, A. and Advani, R.H. (2013) Bruton tyrosine kinase inhibitors: a promising novel
796 targeted treatment for B cell lymphomas, *Br J Haematol*, 163(4), 436-43.

797 Allen, P.M. and Unanue, E.R. (1984) Differential requirements for antigen processing by
798 macrophages for lysozyme-specific T cell hybridomas, *J Immunol*, 132(3), 1077-9.

799 Allman, D. and Pillai, S. (2008) Peripheral B cell subsets, *Curr Opin Immunol*, 20(2), 149-57.

800 Andrews, N.W., Almeida, P.E. and Corrotte, M. (2014) Damage control: cellular mechanisms of
801 plasma membrane repair, *Trends in Cell Biology*, 24(12), 734-42.

802 Bachmann, M.F. and Jennings, G.T. (2010) Vaccine delivery: a matter of size, geometry,
803 kinetics and molecular patterns, *Nat Rev Immunol*, 10(11), 787-96.

804 Bansal, D., Miyake, K., Vogel, S.S., Groh, S., Chen, C.C., Williamson, R., McNeil, P.L. and
805 Campbell, K.P. (2003) Defective membrane repair in dysferlin-deficient muscular dystrophy,
806 *Nature*, 423(6936), 168-72.

807 Batista, F.D. and Harwood, N.E. (2009) The who, how and where of antigen presentation to B
808 cells, *Nat Rev Immunol*, 9(1), 15-27.

809 Batista, F.D., Iber, D. and Neuberger, M.S. (2001) B cells acquire antigen from target cells after
810 synapse formation, *Nature*, 411(6836), 489-94.

811 Batista, F.D. and Neuberger, M.S. (1998) Affinity dependence of the B cell response to antigen:
812 a threshold, a ceiling, and the importance of off-rate, *Immunity*, 8(6), 751-9.

813 Batista, F.D. and Neuberger, M.S. (2000) B cells extract and present immobilized antigen:
814 implications for affinity discrimination, *EMBO J*, 19(4), 513-20.

815 Bresnick, A.R. (1999) Molecular mechanisms of nonmuscle myosin-II regulation, *Curr Opin*
816 *Cell Biol*, 11(1), 26-33.

817 Cheng, P.C., Brown, B.K., Song, W. and Pierce, S.K. (2001) Translocation of the B cell antigen
818 receptor into lipid rafts reveals a novel step in signaling, *J Immunol*, 166(6), 3693-701.

819 Corrotte, M., Cerasoli, M., Maeda, F.Y. and Andrews, N.W. (2020) Endophilin-A2-dependent
820 tubular endocytosis promotes plasma membrane repair and parasite invasion, *J Cell Sci*, 134(5).

821 Cyster, J.G. (2010) B cell follicles and antigen encounters of the third kind, *Nat Immunol*,
822 11(11), 989-96.

823 Demonbreun, A.R., Fallon, K.S., Oosterbaan, C.C., Bogdanovic, E., Warner, J.L., Sell, J.J.,
824 Page, P.G., Quattrocelli, M., Barefield, D.Y. and McNally, E.M. (2019) Recombinant annexin
825 A6 promotes membrane repair and protects against muscle injury, *J Clin Invest*, 129(11), 4657-
826 4670.

827 Diaz, D., Prieto, A., Barcenilla, H., Monserrat, J., Prieto, P., Sánchez, M.A., Reyes, E.,
828 Hernandez-Fuentes, M.P., de la Hera, A., Orfao, A. and Alvarez-Mon, M. (2004) Loss of lineage
829 antigens is a common feature of apoptotic lymphocytes, *J Leukoc Biol*, 76(3), 609-15.

830 Dustin, M.L., Starr, T., Varma, R. and Thomas, V.K. (2007) Supported planar bilayers for study
831 of the immunological synapse, *Curr Protoc Immunol*, Chapter 18, Unit 18.13.

832 Fensome-Green, A., Stannard, N., Li, M., Bolsover, S. and Cockcroft, S. (2007) Bromoenol
833 lactone, an inhibitor of Group V1A calcium-independent phospholipase A2 inhibits antigen-
834 stimulated mast cell exocytosis without blocking Ca2+ influx, *Cell Calcium*, 41(2), 145-53.

835 Fleire, S.J., Goldman, J.P., Carrasco, Y.R., Weber, M., Bray, D. and Batista, F.D. (2006) B cell
836 ligand discrimination through a spreading and contraction response, *Science*, 312(5774), 738-41.

837 Fuchs, H. and Gessner, R. (2002) Iodination significantly influences the binding of human
838 transferrin to the transferrin receptor, *Biochim Biophys Acta*, 1570(1), 19-26.

839 Gitlin, A.D., Shulman, Z. and Nussenzweig, M.C. (2014) Clonal selection in the germinal centre
840 by regulated proliferation and hypermutation, *Nature*, 509(7502), 637-40.

841 Gonzalez, S.F., Degn, S.E., Pitcher, L.A., Woodruff, M., Heesters, B.A. and Carroll, M.C.
842 (2011) Trafficking of B cell antigen in lymph nodes, *Annu Rev Immunol*, 29, 215-33.

843 Hartley, S.B., Crosbie, J., Brink, R., Kantor, A.B., Basten, A. and Goodnow, C.C. (1991)
844 Elimination from peripheral lymphoid tissues of self-reactive B lymphocytes recognizing
845 membrane-bound antigens, *Nature*, 353(6346), 765-9.

846 Ibata, K., Kono, M., Narumi, S., Motohashi, J., Kakegawa, W., Kohda, K. and Yuzaki, M.
847 (2019) Activity-Dependent Secretion of Synaptic Organizer Cbln1 from Lysosomes in Granule
848 Cell Axons, *Neuron*, 102(6), 1184-1198.e10.

849 Jaiswal, J.K., Chakrabarti, S., Andrews, N.W. and Simon, S.M. (2004) Synaptotagmin VII
850 restricts fusion pore expansion during lysosomal exocytosis, *PLoS Biol*, 2(8), E233.

851 Khan, F., Porter, M., Schwenk, R., DeBot, M., Saudan, P. and Dutta, S. (2015) Head-to-Head
852 Comparison of Soluble vs. Qβ VLP Circumsporozoite Protein Vaccines Reveals Selective
853 Enhancement of NANP Repeat Responses, *PLoS One*, 10(11), e0142035.

854 Langley, D.B., Crossett, B., Schofield, P., Jackson, J., Zeraati, M., Maltby, D., Christie, M.,
855 Burnett, D., Brink, R., Goodnow, C. and Christ, D. (2017) Structural basis of antigen
856 recognition: crystal structure of duck egg lysozyme, *Acta Crystallogr D Struct Biol*, 73(Pt 11),
857 910-920.

858 Liu, C., Miller, H., Orlowski, G., Hang, H., Upadhyaya, A. and Song, W. (2012) Actin
859 reorganization is required for the formation of polarized B cell receptor signalosomes in response
860 to both soluble and membrane-associated antigens, *J Immunol*, 188(7), 3237-46.

861 Liu, C.S.C. and Ganguly, D. (2019) Mechanical Cues for T Cell Activation: Role of Piezo1
862 Mechanosensors, *Crit Rev Immunol*, 39(1), 15-38.

863 Liu, C.S.C., Raychaudhuri, D., Paul, B., Chakrabarty, Y., Ghosh, A.R., Rahaman, O., Talukdar,
864 A. and Ganguly, D. (2018) Cutting Edge: Piezo1 Mechanosensors Optimize Human T Cell
865 Activation, *J Immunol*, 200(4), 1255-1260.

866 Malinova, D., Wasim, L., Engels, N. and Tolar, P. (2020) Endophilin A2 regulates B cell protein
867 trafficking and humoral responses, bioRxiv, https://doi.org/10.1101/2020.04.20.050419

868 McNeil, P.L., Miyake, K. and Vogel, S.S. (2003) The endomembrane requirement for cell
869 surface repair, *Proc Natl Acad Sci U S A*, 100(8), 4592-7.

870 Miller, H., Castro-Gomes, T., Corrotte, M., Tam, C., Maugel, T.K., Andrews, N.W. and Song,
871 W. (2015) Lipid raft-dependent plasma membrane repair interferes with the activation of B
872 lymphocytes, *J Cell Biol*, 211(6), 1193-205.

873 Naegeli, K.M., Hastie, E., Garde, A., Wang, Z., Keeley, D.P., Gordon, K.L., Pani, A.M., Kelley,
874 L.C., Morrissey, M.A., Chi, Q., Goldstein, B. and Sherwood, D.R. (2017) 'Cell Invasion In Vivo
875 via Rapid Exocytosis of a Transient Lysosome-Derived Membrane Domain', *Dev Cell*, 43(4),
876 403-417.e10.

877 Natarajan, K., Sahoo, N.C. and Rao, K.V. (2001) Signal thresholds and modular synergy during
878 expression of costimulatory molecules in B lymphocytes, *J Immunol*, 167(1), 114-22.

879 Natkanski, E., Lee, W.Y., Mistry, B., Casal, A., Molloy, J.E. and Tolar, P. (2013) B cells use
880 mechanical energy to discriminate antigen affinities, *Science*, 340(6140), 1587-90.

881 Reddy, A., Caler, E.V. and Andrews, N.W. (2001) Plasma membrane repair is mediated by
882 Ca(2+)-regulated exocytosis of lysosomes, *Cell*, 106(2), 157-69.

883 Reth, M. (1994) B cell antigen receptors, *Curr Opin Immunol*, 6(1), 3-8. Rodríguez, A., Webster,
884 P., Ortego, J. and Andrews, N.W. (1997) Lysosomes behave as Ca2+-regulated exocytic vesicles
885 in fibroblasts and epithelial cells, *J Cell Biol*, 137(1), 93-104.

886 Sagaert, X. and De Wolf-Peeters, C. (2003) Classification of B-cells according to their
887 differentiation status, their micro-anatomical localisation and their developmental lineage,
888 *Immunol Lett*, 90(2-3), 179-86.

889 Shlomchik, M.J. and Weisel, F. (2012) Germinal center selection and the development of
890 memory B and plasma cells, *Immunol Rev*, 247(1), 52-63.
891 Spillane, K.M. and Tolar, P. (2017) B cell antigen extraction is regulated by physical properties
892 of antigen-presenting cells, *J Cell Biol*, 216(1), 217-230.

893 Spillane, K.M. and Tolar, P. (2018) Mechanics of antigen extraction in the B cell synapse, *Mol*
894 *Immunol*, 101, 319-328, available:

895 Suzuki, K., Grigorova, I., Phan, T.G., Kelly, L.M. and Cyster, J.G. (2009) Visualizing B cell
896 capture of cognate antigen from follicular dendritic cells, *J Exp Med*, 206(7), 1485-93.

897 Tam, C., Idone, V., Devlin, C., Fernandes, M.C., Flannery, A., He, X., Schuchman, E., Tabas, I.
898 and Andrews, N.W. (2010) Exocytosis of acid sphingomyelinase by wounded cells promotes
899 endocytosis and plasma membrane repair, *J Cell Biol*, 189(6), 1027-38.

900 Tay, B., Stewart, T.A., Davis, F.M., Deuis, J.R. and Vetter, I. (2019) Development of a high-
901 throughput fluorescent no-wash sodium influx assay, *PLoS One*, 14(3), e0213751.

902 Vidard, L., Kovacsovics-Bankowski, M., Kraeft, S.K., Chen, L.B., Benacerraf, B. and Rock,
903 K.L. (1996) Analysis of MHC class II presentation of particulate antigens of B lymphocytes, *J*
904 *Immunol*, 156(8), 2809-18.

905 Villeneuve, J., Bassaganyas, L., Lepreux, S., Chiritoiu, M., Costet, P., Ripoche, J., Malhotra, V.
906 and Schekman, R. (2018) Unconventional secretion of FABP4 by endosomes and secretory
907 lysosomes, *J Cell Biol*, 217(2), 649-665.

908 Wang, J., Lin, F., Wan, Z., Sun, X., Lu, Y., Huang, J., Wang, F., Zeng, Y., Chen, Y.H., Shi, Y.,
909 Zheng, W., Li, Z., Xiong, C. and Liu, W. (2018) Profiling the origin, dynamics, and function of
910 traction force in B cell activation, *Sci Signal*, 11(542).

911 Wang, J.C., Bolger-Munro, M. and Gold, M.R. (2018) Imaging the Interactions Between B Cells
912 and Antigen-Presenting Cells, *Methods Mol Biol*, 1707, 131-161.

913 Yuseff, M.I., Reversat, A., Lankar, D., Diaz, J., Fanget, I., Pierobon, P., Randrian, V.,
914 Larochette, N., Vascotto, F., Desdouets, C., Jauffred, B., Bellaiche, Y., Gasman, S., Darchen, F.,
915 Desnos, C. and Lennon-Dumenil, A.M. (2011) Polarized secretion of lysosomes at the B cell
916 synapse couples antigen extraction to processing and presentation, *Immunity*, 35(3), 361-74.

917 Zhang, Z., Chen, G., Zhou, W., Song, A., Xu, T., Luo, Q., Wang, W., Gu, X.S. and Duan, S.
918 (2007) Regulated ATP release from astrocytes through lysosome exocytosis, *Nat Cell Biol*, 9(8),
919 945-53.